

Unravelling the causes of the seismicity induced by underground gas storage at Castor, Spain

Víctor Vilarrasa, Silvia de Simone, Jesus Carrera, Antonio Villaseñor

▶ **To cite this version:**

Víctor Vilarrasa, Silvia de Simone, Jesus Carrera, Antonio Villaseñor. Unravelling the causes of the seismicity induced by underground gas storage at Castor, Spain. Geophysical Research Letters, 2021, 48 (7), 10.1029/2020GL092038 . insu-03172897

HAL Id: insu-03172897

https://insu.hal.science/insu-03172897

Submitted on 11 Jun 2021

HAL is a multi-disciplinary open access archive for the deposit and dissemination of scientific research documents, whether they are published or not. The documents may come from teaching and research institutions in France or abroad, or from public or private research centers.

L'archive ouverte pluridisciplinaire **HAL**, est destinée au dépôt et à la diffusion de documents scientifiques de niveau recherche, publiés ou non, émanant des établissements d'enseignement et de recherche français ou étrangers, des laboratoires publics ou privés.



Distributed under a Creative Commons Attribution 4.0 International License

Check for updates

AGU ADVANCING EARTH AND SPACE SCIENCE

Geophysical Research Letters

RESEARCH LETTER
10.1029/2020GL092038

Unraveling the Causes of the Seismicity Induced by Underground Gas Storage at Castor, Spain

Víctor Vilarrasa[1,2,3], Silvia De Simone[1,4], Jesus Carrera[1,3], and Antonio Villaseñor[5]

[1]Institute of Environmental Assessment and Water Research, Spanish National Research Council (IDAEA-CSIC), Barcelona, Spain, [2]Mediterranean Institute for Advanced Studies, Spanish National Research Council (IMEDEA-CSIC), Esporles, Spain, [3]Associated Unit: Hydrogeology Group (UPC-CSIC), Barcelona, Spain, [4]University of Rennes, Centre for Scientific Research, Géosciences Rennes, Rennes, France, [5]Institute of Marine Sciences, Spanish National Research Council (ICM-CSIC), Barcelona, Spain

Key Points:

- Gas injection, through both pore pressure buildup and buoyancy, reactivated mainly aseismically the critically stressed Amposta fault
- Shear slip stress transfer due to creep of the Amposta fault reactivated an unmapped critically stressed fault in the crystalline basement
- Felt earthquakes did not occur until pore pressure reductions had dissipated where shear slip stress transfer led to worsened stability

Supporting Information:

- Supporting Information S1
- Figure S1
- Movie S1

Correspondence to:

V. Vilarrasa,
victor.vilarrasa@idaea.csic.es

Citation:

Vilarrasa, V., De Simone, S., Carrera, J., & Villaseñor, A. (2021). Unraveling the causes of the seismicity induced by underground gas storage at Castor, Spain. *Geophysical Research Letters*, *48*, e2020GL092038. https://doi.org/10.1029/2020GL092038

Received 9 DEC 2020
Accepted 4 MAR 2021

Author Contributions:

Conceptualization: Víctor Vilarrasa, Jesus Carrera
Data curation: Víctor Vilarrasa, Silvia De Simone, Antonio Villaseñor
Formal analysis: Víctor Vilarrasa, Silvia De Simone, Jesus Carrera, Antonio Villaseñor
Funding acquisition: Víctor Vilarrasa, Antonio Villaseñor
Investigation: Víctor Vilarrasa, Silvia De Simone

© 2021. The Authors.
This is an open access article under the terms of the Creative Commons Attribution-NonCommercial License, which permits use, distribution and reproduction in any medium, provided the original work is properly cited and is not used for commercial purposes.

Abstract The offshore Castor Underground Gas Storage (UGS) project had to be halted after gas injection triggered three *M*4 earthquakes, each larger than any ever induced by UGS. The mechanisms that induced seismicity in the crystalline basement at 5–10 km depth after gas injection at 1.7 km depth remain unknown. Here, we propose a combination of mechanisms to explain the observed seismicity. First, the critically stressed Amposta fault, bounding the storage formation, crept by the superposition of well-known overpressure effects and buoyancy of the relatively light injected gas. This aseismic slip brought an unmapped critically stressed fault in the hydraulically disconnected crystalline basement to failure. We attribute the delay between induced earthquakes to the pressure drop associated to expansion of areas where earthquakes slips cause further instabilities. Earthquakes occur only after these pressure drops have dissipated. Understanding triggering mechanisms is key to forecast induced seismicity and successfully design deep underground operations.

Plain Language Summary Underground fluid injection for energy-related activities usually induces microseismicity (not felt earthquakes). But felt earthquakes are sometimes induced, which may cause public concern and project cancellation. This was the case of the offshore Castor underground gas storage (UGS), Spain. Gas injection induced numerous seismic events, including three with magnitudes around 4, larger than any other earthquake ever induced by UGS. These earthquakes occurred after the stop of injection in the crystalline basement, which is hydraulically disconnected from, and significantly deeper than the storage formation. To explain this seismicity, we propose a combination of mechanisms. First, the Amposta fault, bounding the site, crept (failed slowly, aseismically) because of pore pressure buildup induced by injection, which reduces the effective compression stabilizing faults, and stress variations caused by gas buoyancy. Aseismic slip of the Amposta fault provoked underground displacements, which reactivated a critically stressed unmapped fault in the crystalline basement. We attribute the delay between earthquakes of the sequence to rock expansion, and stabilizing pore pressure drop, in areas where slip displacement might cause new earthquakes. Earthquakes occur only after the pressure drop dissipates, which takes some time. Assessing fault stability prior to gas injection would have identified the risk of inducing seismicity.

1. Introduction

The processes that caused the induced seismicity at the Castor underground natural gas storage (UGS) project, Spain, have not been clarified yet. Castor UGS constitutes the largest seismicity induced worldwide in an UGS ($M > 4$) and represents the case of project cancellation resulting from induced or triggered seismicity with the highest cost ever. The cancellation of the project implies an investment compensation to the operating company that may cost up to 4.73 billion euros to Spanish citizens (The Corner, 2017). Although the compensation has been paid with public money, data gathered by the operating company through the drilling of 14 wells and several characterization campaigns have not been made publicly available, which hampers the scientific community from analyzing what caused the induced seismicity at Castor UGS.

Cushion gas injection at Castor UGS induced a sequence of felt earthquakes during September–October 2013 (Figure 1a and Movie S1), leading to the project cancellation before entering into operation. Despite

Methodology: Víctor Vilarrasa, Silvia De Simone, Jesus Carrera, Antonio Villaseñor
Project Administration: Víctor Vilarrasa, Silvia De Simone, Antonio Villaseñor
Software: Víctor Vilarrasa, Silvia De Simone, Antonio Villaseñor
Validation: Víctor Vilarrasa, Silvia De Simone
Visualization: Victor Vilarrasa, Silvia De Simone, Antonio Villaseñor
Writing – original draft: Víctor Vilarrasa, Silvia De Simone
Writing – review & editing: Víctor Vilarrasa, Silvia De Simone, Jesus Carrera, Antonio Villaseñor

the offshore platform being more than 20 km away from the coast, the local population felt a large number of earthquakes during 20 days after the stop of cushion gas injection into a depleted oil field at 1.7 km depth. Each of the three largest earthquakes, with magnitudes 4.08, 4.01, and 3.97, constitute the largest seismicity induced worldwide in an UGS. The earthquake locations are uncertain, with the hypocenters appearing to be deep (>5 km depth) when using the most detailed seismic velocity model available for this region (Villaseñor et al., 2020), whereas previous studies suggest shallower depths (Cesca et al., 2014; Juanes et al., 2017). The uncertainty in earthquake location is caused by a poor monitoring network, with a scarce number of seismometers near the area and an inhomogeneous distribution in space, with all of them located inland given the absence of ocean-bottom seismometers (Cesca et al., 2014; Gaite et al., 2016; Juanes et al., 2017).

The few previous studies on this site include both statistical and physics-based approaches. On the one hand, the statistical analysis of the sequence shows a decrease in the b-value of the Gutenberg-Richter law (Gutenberg & Richter, 1942) after the stop of injection, indicating a tendency to induce larger events in the post-injection period (Ruiz-Barajas et al., 2017). Such tendency is not novel in fluid injection operations as it has also been observed in other induced earthquake sequences, like at the Soultz-sous-Forêts, France (Cuenot et al., 2008) and Basel, Switzerland (Bachmann et al., 2011) deep geothermal projects. On the other hand, physics-based models can shed light on the mechanisms controlling such increase of magnitude after shut-in. Juanes et al. (2017) used numerical simulations to show that the critically stressed Amposta fault, which bounds the storage formation, was destabilized by gas injection. However, they limited their analysis

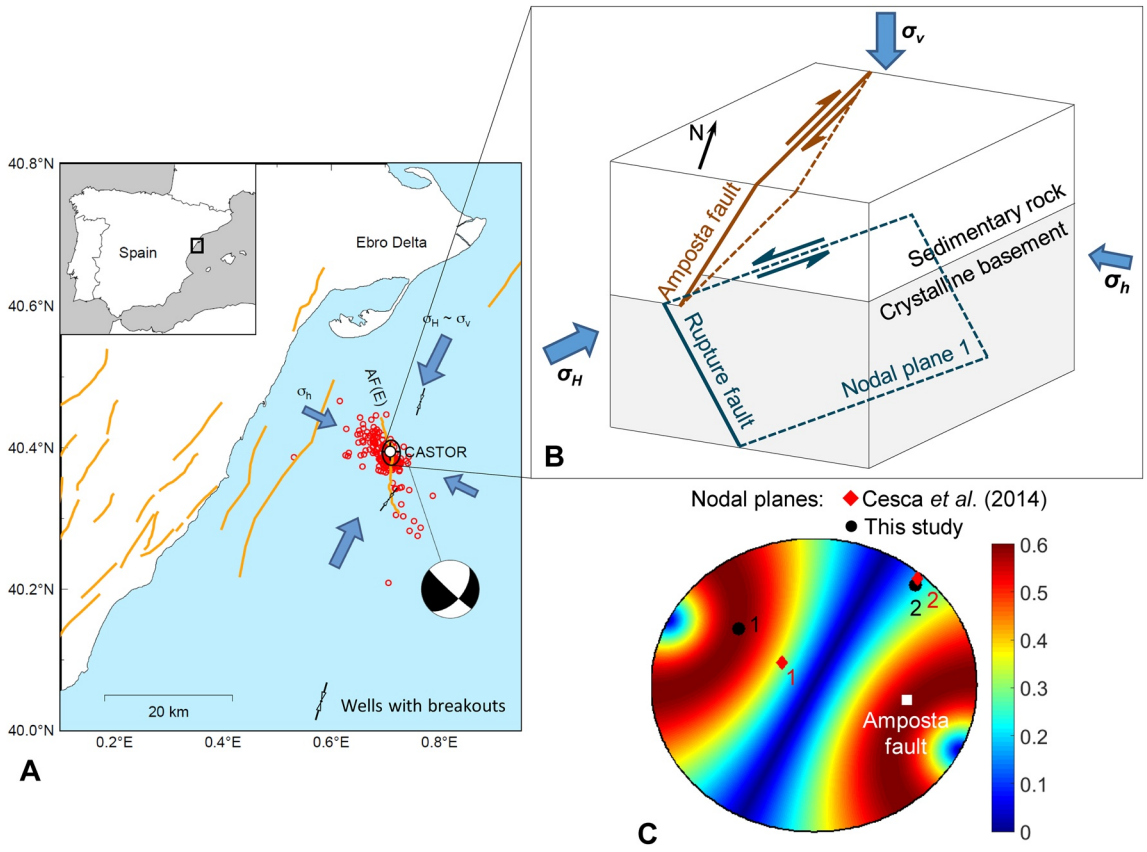


Figure 1. (a) Location map of the Castor platform, including the traces at the surface or sea bottom of the faults in the vicinity of the site (AF(e) indicates the East Amposta Fault), the location of the wells used to estimate the stress tensor from breakouts, the location of the induced seismicity, the beach ball with the nodal planes of the largest earthquakes (the nodal planes of the other induced earthquakes are similar) and the estimated stress tensor (b) schematic representation of the Amposta fault and the rupture fault within the crystalline basement and their orientation with respect to the stress tensor; and (c) slip tendency stereo plot of the Castor storage formation prior to injection. The red diamonds and black dots correspond, respectively, to the nodal planes derived by Cesca et al. (2014) and those used in this study. The white square indicates the Amposta fault, which lays on the critically stressed area (red colors corresponding to a mobilized friction coefficient of 0.6) and thus, the fault may undergo shear failure for small perturbations of the effective stress state.

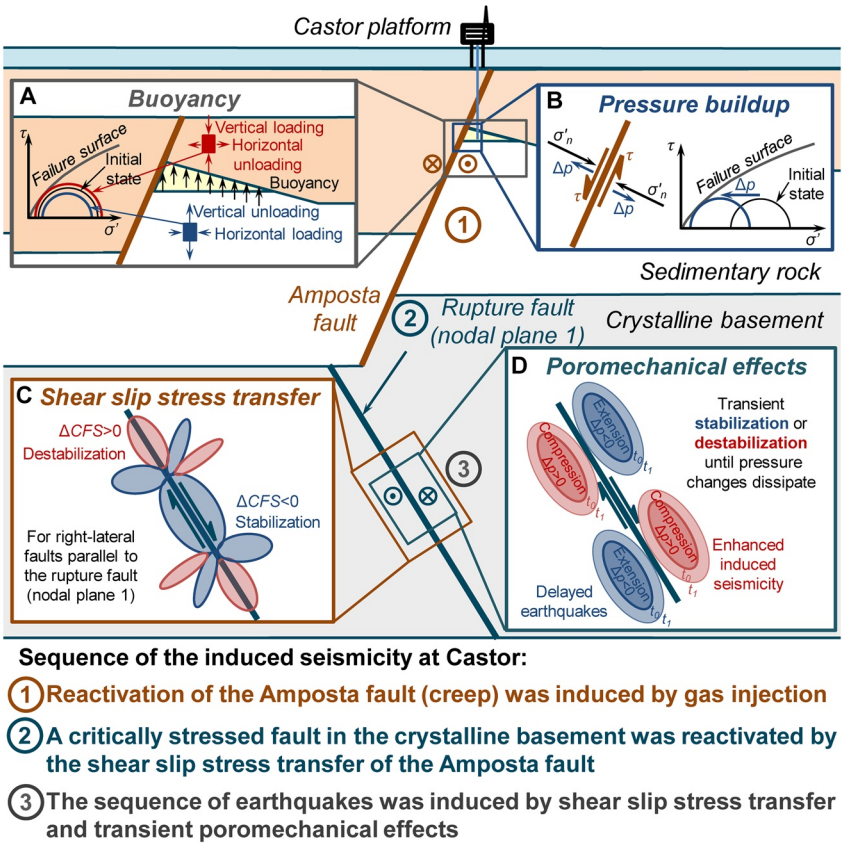


Figure 2. Proposed sequence and mechanisms leading to induced seismicity at Castor. First, the injection of cushion gas aseismically reactivated the Amposta fault because of the combined effect of (a) buoyancy and (b) pressure buildup. The stress transfer caused by the aseismic slip of the Amposta fault reactivated a critically stressed fault in the crystalline basement, which induced the sequence of earthquakes by (c) shear slip stress transfer, which (d) leads to volumetric expansion and pore pressure drops in the zones where slip transfer is destabilizing, delaying new earthquakes until these drops have dissipated.

to the injection period and do not explain the largest deep seismic events occurring in the post-injection stage. In contrast, Saló et al. (2017) focused the analysis on the post-injection period, finding that shear slip stress transfer may have contributed to trigger subsequent events. However, the link between gas injection and the subsequent deep earthquakes is still missing.

Unraveling the peculiarity of the Castor induced earthquakes requires addressing the following open scientific questions. (i) How can the injection of gas into a shallow sedimentary formation induce deep earthquakes into the crystalline basement if they are hydraulically disconnected? (ii) Can the buoyancy of the injected gas contribute to fault reactivation? (iii) Why did the main earthquakes occur after the stop of injection? (iv) What is the cause of delay between earthquakes that are induced by shear slip stress transfer?

By answering these questions, we aim at finding the triggering mechanisms that induced the sequence of felt earthquakes at Castor. We conjecture that the critically stressed Amposta fault bounding the storage formation was destabilized not only by the traditional pressure buildup, which was small in this case because of the high permeability of the storage formation, but also by buoyancy forces induced by gas injection. As a result, the Amposta fault creeped, progressively accumulating aseismic slip and transferring stress to the crystalline basement, where a critically stressed fault reached failure conditions a few days after the stop of injection, triggering the first felt earthquake. The rest of the felt earthquakes of the sequence were induced by shear slip stress transfer. The interevent times between these earthquakes could be explained by the transient poromechanical pressure changes resulting from shear slip. A schematic summary of the proposed combination of mechanisms is presented in Figure 2.

2. Castor Setting

The Castor UGS is located in the Valencia Through, off the coast of northeastern Spain, which was formed due to a rifting phase during Neogene times with a NW–SE extension direction (Roca & Guimerà, 1992) (Figure 1a). The minimum horizontal stress roughly coincides with the direction of extension. The orientation of the maximum horizontal stress follows a NE–SW direction in the northern part of the Valencia Trough, but it rotates to a NNE–SSW orientation in the southern part (Jurado & Müller, 1997), where the Castor UGS is located. Since there are no data available on the stress state at Castor, we refer to the estimates based on breakouts of two wells (Delta E-3 and San Carlos III/1) placed some 10 km away from the Castor UGS (Figure 1a), which are characterized by a normal faulting/strike-slip stress regime, that is, the vertical stress is equal to the maximum horizontal stress (Schindler et al., 1998). The mean azimuth of the maximum horizontal stress is 26.35° ± 11.75°. The stress state at a depth of 1.7 km, that is, the depth of the storage formation, is estimated to have the vertical and maximum horizontal effective stresses equal to 20.5 MPa, the minimum horizontal effective stress equal to 6.6 MPa and the pore pressure equal to 17.0 MPa. This evaluation is based on assuming a rock density of 2250 kg/m^3, a fault friction coefficient of 0.6 (Bakker et al., 2016; Barton, 1976), hydrostatic pore pressure and taking into account that the Valencia Through is an active seismic zone (Perea et al., 2012) and, thus, that favorably oriented faults are critically stressed.

The storage formation is an oil-bearing tilted limestone formation dipping 7° to the East, which underwent oil production in the 1970s and 1980s with no reported felt induced seismicity (Batchelor et al., 2007; Seeman et al., 1990). The storage formation, which is highly fractured and karstified (Playà et al., 2010), is bounded to the West by the East Amposta fault, a NNE–SSW normal fault that dips to the West with an angle of 60° (Perea et al., 2012) (Figure 1b). The fault offset equals 1 km (Batchelor et al., 2007), which suggests a low-permeability resulting from accumulation of clay-rich geomaterials in the fault core over successive shear slip events (Egholm et al., 2008). According to this setting and the estimated initial stress state, the slip tendency analysis reveals that the Amposta fault is critically stressed assuming a typical friction coefficient of 0.6 (Figure 1c). There are little data on the rock types below the storage formation down to the crystalline basement, which is found around 5 km depth. Available data down to 2.25 km depth show alternations of low and high permeability layers (Schindler et al., 1998). The presence of low-permeability rock below the storage formation impedes hydraulic connection with the crystalline basement.

3. Potential Triggering Mechanisms

3.1. Pressure Buildup and Buoyancy Destabilize the Amposta Fault

A total of $1.02{\cdot}10^8$ m^3 of natural gas at standard conditions were injected from the September 2, 2013 to September 16, 2013 as cushion gas, inducing hundreds of co-injection microseismic events (Cesca et al., 2014; Gaite et al., 2016). According to the operating company, the pressure buildup was lower than 0.8 MPa, implying a reservoir permeability higher than 10^{-12} m^2, a plausible value for a karstic reservoir (Seeman et al., 1990). The injected gas has a density around 100 kg/m^3 at reservoir conditions, that is, 178 bar and 80°C, which implies a difference of some 900 kg/m^3 between the gas and the resident pore water densities. We analyze the effect of both pressure buildup and buoyancy on the stability of the Amposta fault by means of coupled two-phase flow and geomechanical numerical simulations (Vilarrasa et al., 2020) (Figure S1) using the finite element method fully coupled simulator CODE_BRIGHT (Olivella et al., 1996) (see SI for details).

Simulation results show that the pore pressure buildup caused by gas injection could reactivate the Amposta fault during injection because of the reduction in the effective stress (Figure 2b). However, pressure buildup alone cannot explain why the largest earthquakes occurred in the post-injection period, because pore pressure rapidly dissipates after shut-in. In contrast, the buoyant injected gas causes a permanent effect (Figure S2a). Buoyancy induces a small increase of the vertical total stress above the storage formation, of 0.08 MPa (Equation S4), and a consequent slight reduction of the horizontal total stresses to satisfy stress equilibrium. These stress changes increase the deviatoric stress in a normal faulting/strike-slip stress regime like the one at Castor, causing failure in critically stressed faults (Figure 2a). Therefore, buoyancy should be considered as a potential triggering mechanism when injecting low-density fluids.

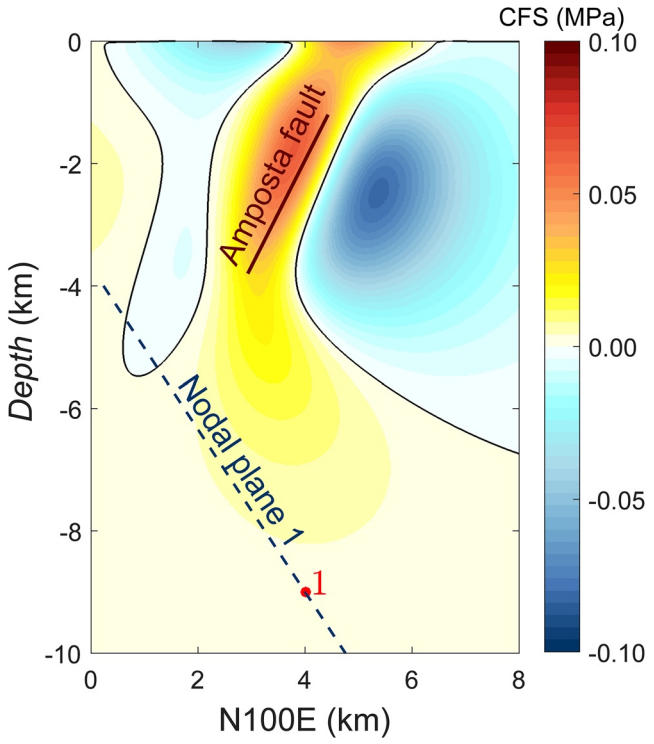


Figure 3. Onset of $M \gtrsim 3.5$ seismicity resulting from the stress transfer induced by the Amposta aseismic slip. Coulomb Failure Stress (*CFS*) at a vertical plane that contains the hypocenter of the first $M \gtrsim 3.5$ earthquake of the sequence (EQ1, red dot) and is perpendicular to the Amposta fault. The black line indicates the 0 isoline. The dark red line represents the projection of the Amposta fault on the plane and the dashed dark blue line represents the projection of the nodal plane 1.

Note that these effects are consistent with the lack of seismicity during the oil production period. In this period, pore pressure was reduced and oil was displaced by water, which is slightly denser.

3.2. Aseismic Slip of the Amposta Fault Triggers the Seismicity Onset in the Deep Basement

Coupled two-phase flow and geomechanical modeling shows that the Amposta fault underwent shear failure conditions during the injection and post injection periods as a result of the combined effect of pore pressure buildup and buoyancy (Figure S2b). Since none of the events for which we have available focal mechanisms coincide with the Amposta fault (Villaseñor et al., 2020), shear slip in the Amposta fault had to occur aseismically as a result of creep. At the mesoscale in rock laboratories, injection-induced aseismic slip has been observed to trigger microseismicity away from the pressurized region as a result of stress transfer (Bhattacharya & Viesca, 2019; Cappa et al., 2019; Duboeuf et al., 2017; Guglielmi et al., 2015). This effect has also been observed at a larger scale in the 2012 Brawley swarm (Wei et al., 2015) and in a swarm induced by hydraulic fracturing in western Canada (Eyre et al., 2020). Thus, aseismic slip could explain the link between fluid injection at shallow depths and the deep induced seismicity observed in the hydraulically disconnected crystalline basement.

We have estimated the stress changes induced by aseismic slip at the Amposta fault using Okada's (Okada, 1992) solution. Given the uncertainty in the length and width of the rupture area, the location of the hypocenter and the rake of the rupture, we have performed an optimization to determine the parameters that better explain the onset of the felt seismicity at depth (see SI for details on the optimization procedure and Figure S6). Assuming that the accumulated aseismic slip in the Amposta fault is of 10 cm, the optimized rupture length and width are 750 and 3,000 m, respectively, with the hypocenter placed to the South of the Castor UGS at a depth of 2.5 km. Thus, the Amposta fault slips from 1.2 to 3.8 km deep, which roughly corresponds to those depths where shear failure is predicted by the coupled fluid flow and geomechanical model (Figure S2b). The slip rake resulting from the optimization is 180°, that is, the fault undergoes a right-lateral slip, which is compatible with the orientation of the Amposta fault with respect to the in situ stress state (Figure 1b).

This right-lateral slip displaces the hanging wall toward the North and the footwall toward the South, where the hypocenter of the first $M > 3$ earthquake of the sequence is located. By observing the stress changes at a vertical plane that is perpendicular to the Amposta fault and that contains the hypocenter of the first earthquake for which we could obtain focal mechanisms, corresponding to $M \gtrsim 3.5$ (Figure S4), compression occurs in the footwall and extension in the hanging wall at the depths where aseismic slip occurs, that is, up to 4 km depth. At deeper depths, the stress in the direction sub-parallel to the minimum principal stress decreases, and the other principal stresses either increase (vertical direction) or remain nearly constant (direction sub-parallel to the maximum horizontal stress). Thus, the deviatoric stress slightly increases, causing the rupture of the fault that coincides with the nodal plane 1, as indicated by the positive Coulomb Failure Stress (*CFS*) at the location of the hypocenter of the first $M \gtrsim 3.5$ earthquake of the sequence (Figure 3).

3.3. Shear Slip Stress Transfer Drives the Earthquake Sequence

The aseismic slip of the Amposta fault brought a critically stressed pre-existing fault in the crystalline basement to failure, triggering the first $M \gtrsim 3.5$ event of the sequence (Figure 3). We apply again the solution of Okada (1992) to calculate the stress variations induced by the slip of each earthquake and assess whether the seismic sequence could be the result of accumulated shear slip stress transfer. We focus on the cluster

of earthquakes for which we have focal mechanisms that is localized below the Castor platform (8 earthquakes) and disregard another cluster of earthquakes that occurred laterally some 9 km to the SE of the Castor platform (5 earthquakes) (see Fig. S3). The mean strike, dip and rake of the selected cluster of earthquakes are 40°, 62.5°, and −5°, respectively, for the nodal plane 1, and 132°, 85.5°, and −152°, respectively, for the nodal plane 2 (Table S2) (Villaseñor et al., 2020).

The nodal plane 2 is a vertical plane oriented NW–SE, roughly perpendicular to the maximum horizontal stress, implying that the shear stress acting on this plane is extremely low, which makes it a very stable plane (Figure 1c). In contrast, the plane corresponding to the nodal plane 1 (oriented NE–SW) dips 62.5° to the East and is almost perpendicular to the minimum horizontal principal stress, which makes it a critically stressed plane in the normal-faulting/strike-slip stress regime at Castor (Figure 1c). Given this stress regime, the slip has a horizontal component, which yields a left-lateral displacement (Figure 1b). This displacement is in agreement with the measured rake of the earthquakes, that is, −5°. When observing the hypocenters at a vertical plane that is perpendicular to the strike of the nodal plane 1, six out of the eight earthquakes align along a plane with the same dip as this nodal plane (Figure S3), indicating that most of the seismicity at Castor occurred in a steeply dipping fault within the crystalline basement. Note that the nodal planes provided by Cesca et al. (2014) cannot explain the sequence of earthquakes (Figure 1c and see SI for further details).

We evaluate, for each earthquake, whether the cumulative stress variation caused by shear slips occurring on nodal plane 1 (Table S2) leads to shear failure conditions at the subsequent hypocenter in the sequence. We assign the values of the slipping surface and the amount of slip according to the magnitude of each event and to the result of an optimization analysis (see SI). We find that the value of the width to length ratio of the slipping surface, W/L, which better explains the sequence is 1.75 (Figure S5 and S7). By assuming this value, indeed, we calculate a $CFS > 0$ at most of the hypocenters as a result of the accumulated stress transfer (Figure S5). Thus, consequent to the aseismic failure of the Amposta fault, a mechanism of shear slip stress transfer has driven the sequence of the $M \gtrsim 3.5$ induced earthquakes that are located below the Castor UGS (Figure 2c).

3.4. Transient Slip-Induced Poromechanical Pressure Changes Cause Delay Between Earthquakes

Shear slip stress transfer occurs immediately after an earthquake is nucleated. However, $M \gtrsim 3.5$ earthquakes in the sequence are triggered at intervals that range from hours to days. This delay can be explained by transient poromechanical pore pressure changes induced by slip (Figure 2d), which we investigate by means of numerical coupled hydro-mechanical simulations (see Section S1.3 in SI for details). Slip compresses the rock ahead of the rupture area in the direction of slip (Figure S9), inducing a pore volume decrease. In contrast, the rock behind the rupture area in the direction of slip undergoes tension, causing an increase in the pore volume and, thus, a decrease in pore pressure. Given that the characteristic time of earthquake slip is much shorter than that of fluid diffusion (Equation S7), pore volume changes induce non-negligible pore pressure changes (of some tens of MPa), that is, undrained response, which modify the effective stresses (Figure S9). While the pressure buildup in the compressed regions may promote shear failure and more seismic events, the pressure drop occurs in the extended regions, which causes a transient improvement in fault stability because these regions would be the most unstable if pore pressure changes were disregarded (Figure. 2d and Figure S10). Seismicity is delayed until these pore pressure changes are dissipated.

Slip-induced poromechanical pressure changes cause transient stability changes around a fault (Figure 4). Where pore pressure drops right after slip, fault stability initially improves, but decreases with time as pore pressure changes dissipate. Eventually, a part of this region reaches failure conditions, explaining the delay between earthquakes of the sequence. The velocity at which pore pressure changes dissipate and thus, the timing between earthquakes, is controlled by hydraulic diffusivity.

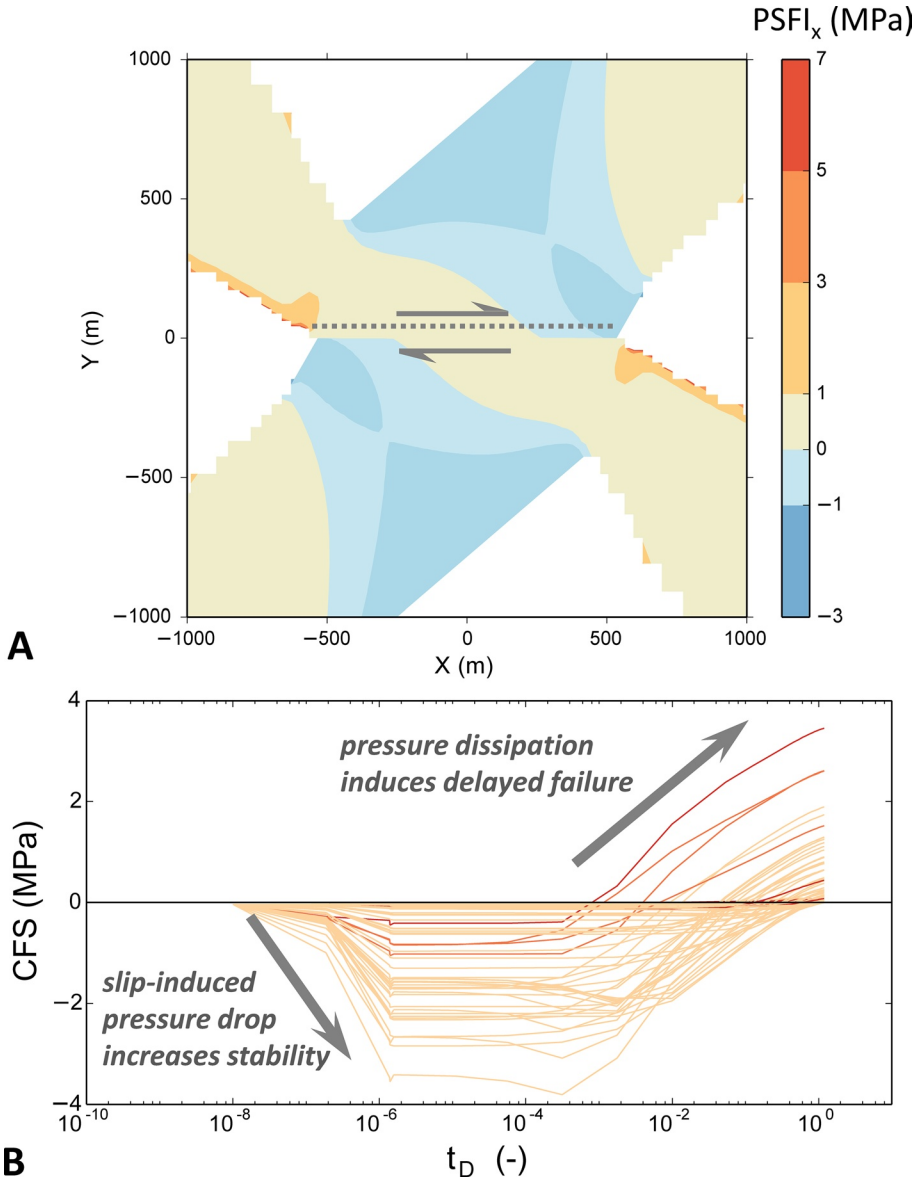


Figure 4. Effect of shear slip-induced pore pressure changes on the stability of a fault placed at 9 km depth, with strike 40° and dip 62.5° (a) Post-Slip HM Failure Index (*PSFI*) (Equation S8, see SI) at dimensionless time $t_D = 1$, that is, once the pressure has dissipated, but the effects of shear slip stress transfer remain. White color indicates the regions that fail during slip; negative values correspond to regions where stability improves after pore pressure dissipation; values between 0 and 1 represent the regions where stability decreases after pore pressure dissipation, but failure conditions are not reached; and values higher than one show the regions where failure occurs after dissipation of the shear slip-induced pore pressure changes (b) Temporal evolution of the Coulomb Failure Stress (*CFS*) at the regions that undergo delayed failure (where *PSFI_x* > 1). Lines correspond to different elements in the domain. Time is normalized with respect to the diffusive characteristic time (Equation S7). Both *PSFI* and *CFS* refer to failure along the direction parallel to the fault.

4. Discussion

Minimizing induced seismicity, particularly large felt earthquakes, is crucial for a successful deployment of geo-energy projects, both because felt events have a negative effect on public perception and because large events may jeopardize well stability and adjacent infrastructure (Langenbruch et al., 2020). First, transparency and data sharing are necessary to achieve a positive public perception. Additionally, thorough site characterization and continuous monitoring are a requirement to reduce subsurface uncertainty and

perform real-time risk assessment of induced seismicity. Unfortunately, Castor was not characterized by these principles.

Site characterization at Castor would have allowed, through fault stability analysis, to identify that the risk of inducing seismicity was very high because the Amposta fault is critically stressed (Figure 1c). In general, sedimentary rocks are not critically stressed because of their low stiffness compared with the stiff crystalline basement, which makes them accumulate less stress (Vilarrasa & Carrera, 2015a). However, sedimentary rocks are critically stressed in some regions, like in the Valencia Through, which is an active seismic region. An accurate estimation of the stress state is essential to limit pore pressure buildup below a threshold to prevent induced seismicity (Vilarrasa & Carrera, 2015b; Zoback & Gorelick; 2015) (Figure 2b).

Apart from pressure buildup, other triggering mechanisms may induce seismicity (Brown & Ge, 2018; Jiang et al., 2020; Vilarrasa et al., 2019). In particular, buoyancy need to be considered when gases are injected because their density is lower than that of water, which generates buoyancy-induced stress redistribution around the storage formation (Figure 2a). Density effects are suspected to have a persistent local effect in seismicity induced by wastewater disposal (Pollyea et al., 2020). At Castor, the combined effect of pressure buildup and buoyancy reactivated the critically stressed Amposta fault, inducing aseismic slip. The aseismic slip rate resulting from our calculations is 0.05 μm/s, which falls within the range of aseismic slip rates reported in the literature. Guglielmi et al. (2015) measured an aseismic slip rate of 0.43 μm/s in a highly monitored injection test at the Laboratoire Souterrain à Bas Bruit, in France, and Wei et al. (2015) estimated an aseismic slip rate of 0.008 μm/s as a result of geothermal operations in Brawley, California.

We have shown that aseismic slip can be a triggering mechanism of induced earthquakes that nucleate in geological formations that are hydraulically disconnected from the injection formation. When aseismic slip occurs, large post-injection seismic events may be induced, as occurred at Soultz-sous-Forêts, France (Cornet et al., 1997) and Le Mayet de Montagne, France (Cornet, 2012). However, at these sites, induced events occurred within the rock mass affected by pressure buildup. Such post-injection seismicity may be explained by a superposition of a destabilizing effect of aseismic slip and a stabilizing effect of the poromechanical response to pressure buildup that compresses faults but vanishes after the stop of injection (De Simone et al., 2017). At Castor, the poromechanical stabilizing effect did not act directly during injection because the crystalline basement was not hydraulically connected with the storage formation. Thus, the delay in the onset of earthquakes after shut-in may have been caused by the progressive accumulation of aseismic slip as the Amposta fault was destabilized by buoyancy.

Once an unmapped critically stressed fault in the crystalline basement was reactivated as a result of aseismic slip of the Amposta fault, a sequence of earthquakes was triggered by shear slip stress transfer (Figure 2c and Figure S5). We argue that the delay between successive earthquakes in the basement is due to fluid diffusion, which dissipates pore pressure changes caused by the poromechanical response to shear slip (Figure 2d). In particular, there are regions where failure is promoted as a result of shear slip stress transfer, but the transient pore pressure drop associated to the fast slip compensates the decrease in stability. Failure conditions are met only when pore pressure is recovered, leading to a new induced earthquake (Figure 4).

5. Conclusions

Castor is a unique and challenging case study that has allowed us to identify a novel combination of triggering mechanisms with the potential to induce earthquakes far away from the region affected by pressure buildup. Buoyancy and aseismic slip stress transfer act as primary mechanisms that trigger the sequence in a hydraulically disconnected and critically stressed pre-existing fault. Then, shear slip stress transfer and the associated slip-induced poromechanical pressure changes trigger the rest of the earthquakes in the sequence. It does not escape to us that these findings may have ground-breaking implications to both induced and natural seismicity forecasting.

Data Availability Statement

The associated data is available at the repository DIGITAL.CSIC (https://digital.csic.es/handle/10261/216863)

Acknowledgments
The authors would like to acknowledge Álvaro González for sharing the catalogs that were used in Cesca et al. (2014). Funding: Víctor Vilarrasa acknowledges funding from the European Research Council (ERC) under the European Union's Horizon 2020 Research and Innovation Program through the Starting Grant GEoREST (www.georest.eu) (grant agreement No. 801809). Antonio Villaseñor acknowledges funding from Spanish Ministry of Science and Innovation grant CGL2017-88864-R. IDAEA-CSIC is a Center of Excellence Severo Ochoa (Spanish Ministry of Science and Innovation, Project CEX2018-000794-S). ICM-CSIC is a Center of Excellence Severo Ochoa (Spanish Ministry of Science and Innovation, Project CEX2019-000928-S).

References

Bachmann, C. E., Wiemer, S., Woessner, J., & Hainzl, S. (2011). Statistical analysis of the induced Basel 2006 earthquake sequence: Introducing a probability-based monitoring approach for Enhanced Geothermal Systems. *Geophysical Journal International*, *186*(2), 793–807. https://doi.org/10.1111/j.1365-246x.2011.05068.x

Bakker, E., Hangx, S. J. T., Niemeijer, A. R., & Spiers, C. J. (2016). Frictional behavior and transport properties of simulated fault gouges derived from a natural CO_2 reservoir. *International Journal of Greenhouse Gas Control*, *54*, 70–83. https://doi.org/10.1016/j.ijggc.2016.08.029

Barton, N. (1976). The shear strength of rock and rock joints. *International Journal of Rock Mechanics and Mining Science & Geomechanics Abstracts*, *13*(9), 255–279. https://doi.org/10.1016/0148-9062(76)90003-6

Batchelor, J. A., Sherley, B., Klepacki, D., Lewis, R., & Jensen, R. E. (2007). Validating the integrity of the Amposta structure for gas storage offshore Spain. In *Proceedings of the offshore Europe, September 4-7, Aberdeen*. Society of Petroleum Engineers. Manuscript 108247.

Bhattacharya, P., & Viesca, R. C. (2019). Fluid-induced aseismic fault slip outpaces pore-fluid migration. *Science*, *364*(6439), 464–468. https://doi.org/10.1126/science.aaw7354

Brown, M. R. M., & Ge, S. (2018). Small earthquakes matter in injection-induced seismicity. *Geophysical Research Letters*, *45*(11), 5445–5453. https://doi.org/10.1029/2018gl077472

Cappa, F., Scuderi, M. M., Collettini, C., Guglielmi, Y., & Avouac, J. P. (2019). Stabilization of fault slip by fluid injection in the laboratory and in situ. *Science Advances*, *5*(3), eaau4065. https://doi.org/10.1126/sciadv.aau4065

Cesca, S., Grigoli, F., Heimann, S., González, Á., Buforn, E., Maghsoudi, S., et al. (2014). The 2013 September–October seismic sequence offshore Spain: A case of seismicity triggered by gas injection? *Geophysical Journal International*, *198*(2), 941–953. https://doi.org/10.1093/gji/ggu172

Cornet, F. H. (2012). The relationship between seismic and aseismic motions induced by forced fluid injections. *Hydrogeology Journal*, *20*, 1463–1466. https://doi.org/10.1007/s10040-012-0901-z

Cornet, F. H., Helm, J., Poitrenaud, H., & Etchecopar, A. (1997). Seismic and aseismic slips induced by large-scale fluid injections. *Pure and Applied Geophysics*, *150*(3–4), 563–583. https://doi.org/10.1007/s000240050093

Cuenot, N., Dorbath, C., & Dorbath, L. (2008). Analysis of the microseismicity induced by fluid injections at the EGS Site of Soultz-sous-Forêts (Alsace, France): Implications for the characterization of the geothermal reservoir properties. *Pure And Applied Geophysics*, *165*(5), 797–828. https://doi.org/10.1007/s00024-008-0335-7

De Simone, S., Carrera, J., & Vilarrasa, V. (2017). Superposition approach to understand triggering mechanisms of post-injection induced seismicity. *Geothermics*, *70*, 85–97. https://doi.org/10.1016/j.geothermics.2017.05.011

Duboeuf, L., De Barros, L., Cappa, F., Guglielmi, Y., Deschamps, A., & Seguy, S. (2017). Aseismic motions drive a sparse seismicity during fluid injections into a fractured zone in a carbonate reservoir. *Journal of Geophysical Research Solid Earth*, *122*(10), 8285–8304. https://doi.org/10.1002/2017jb014535

Egholm, D. L., Clausen, O. R., Sandiford, M., Kristensen, M. B., & Korstgård, J. A. (2008). The mechanics of clay smearing along faults. *Geology*, *36*(10), 787–790. https://doi.org/10.1130/g24975a.1

Eyre, T. S., Zecevic, M., Salvage, R. O., & Eaton, D. W. (2020). A long-lived swarm of hydraulic fracturing-induced seismicity provides evidence for aseismic slip. *Bulletin of the Seismological Society of America*, *110*(5), 2205. https://doi.org/10.1785/0120200107

Gaite, B., Ugalde, A., Villaseñor, A., & Blanch, E. (2016). Improving the location of induced earthquakes associated with an underground gas storage in the Gulf of Valencia (Spain). *Physics of the Earth and Planetary Interiors*, *254*, 46–59. https://doi.org/10.1016/j.pepi.2016.03.006

Guglielmi, Y., Cappa, F., Avouac, J.-P., Henry, P., & Elsworth, D. (2015). Seismicity triggered by fluid injection-induced aseismic slip. *Science*, *348*(6240), 1224–1226. https://doi.org/10.1126/science.aab0476

Gutenberg, B., & Richter, C. F. (1942). Earthquake magnitude, intensity, energy, and acceleration. *Bulletin of the Seismological Society of America*, *32*(3), 163–191.

Jiang, G., Qiao, X., Wang, X., Lu, R., Liu, L., Yang, H., et al. (2020). GPS observed horizontal ground extension at the Hutubi (China) underground gas storage facility and its application to geomechanical modeling for induced seismicity. *Earth and Planetary Science Letters*, *530*, 115943. https://doi.org/10.1016/j.epsl.2019.115943

Juanes, R., Castiñeira, D., Fehler, M. C., Hager, B. H., Jha, B., Shaw, J. H., & Plesch, A. (2017). *Coupled flow and geomechanical modeling, and assessment of induced seismicity, at the Castor Underground Gas Storage Project. Final Report*, April 2017. Retrieved from http://www.minetad.gob.es/es-ES/GabinetePrensa/NotasPrensa/2017/Paginas/informe-castor20170503.aspx (Accessed on May 5, 2017).

Jurado, M.-J., & Müller, B. (1997). Contemporary tectonic stress in northeastern Iberia. New results from borehole breakout analysis. *Tectonophysics*, *282*(1), 99–115. https://doi.org/10.1016/s0040-1951(97)00214-x

Langenbruch, C., Ellsworth, W. L., Woo, J. U., & Wald, D. J. (2020). Value at induced risk: Injection-induced seismic risk from low-probability, high-impact events. *Geophysical Research Letters*, *47*(2), e2019GL085878. https://doi.org/10.1029/2019gl085878

Okada, Y. (1992). Internal deformation due to shear and tensile faults in a half-space. *Bulletin of the Seismological Society of America*, *82*(2), 1018–1040.

Olivella, S., Gens, A., Carrera, J., & Alonso, E. E. (1996). Numerical formulation for a simulator (CODE_BRIGHT) for the coupled analysis of saline media. *Engineering Computations*, *13*(7), 87–112. https://doi.org/10.1108/02644409610151575

Perea, H., Masana, E., & Santanach, P. (2012). An active zone characterized by slow normal faults, the northwestern margin of the València trough (NE Iberia): A review. *Journal of Iberian Geology*, *38*(1), 9–30. https://doi.org/10.5209/rev_jige.2012.v38.n1.39204

Playà, E., Travé, A., Caja, M. A., Salas, R., & Martín-martín, J. D. (2010). Diagenesis of the Amposta offshore oil reservoir (Amposta Marino C2 well, Lower Cretaceous, Valencia Trough, Spain). *Geofluids*, *10*(3), 314–333. https://doi.org/10.1111/j.1468-8123.2009.00266.x

Pollyea, R. M., Konzen, G. L., Chambers, C. R., Pritchard, J. A., Wu, H., & Jayne, R. S. (2020). A new perspective on the hydraulics of oilfield wastewater disposal: How PTX conditions affect fluid pressure transients that cause earthquakes. *Energy & Environmental Science*, *13*(9), 3014–3031. https://doi.org/10.1039/d0ee01864c

Roca, E., & Guimerà, J. (1992). The Neogene structure of the eastern Iberian margin: Structural constraints on the crustal evolution of the Valencia trough (western Mediterranean). *Tectonophysics*, *203*(1–4), 203–218. https://doi.org/10.1016/0040-1951(92)90224-t

Ruiz-Barajas, S., Sharma, N., Convertito, V., Zollo, A., & Benito, B. (2017). Temporal evolution of a seismic sequence induced by a gas injection in the Eastern coast of Spain. *Scientific Reports*, *7*(1), 1–15. https://doi.org/10.1038/s41598-017-02773-2

Saló, L., Frontera, T., Goula, X., Pujades, L. G., & Ledesma, A. (2017). Earthquake static stress transfer in the 2013 Gulf of Valencia (Spain) seismic sequence. *Solid Earth*, *8*(5), 857. https://doi.org/10.5194/se-8-857-2017

Schindler, A., Jurado, M.-J., & Müller, B. (1998). Stress orientation and tectonic regime in the northwestern Valencia Trough from borehole data. *Tectonophysics*, *300*(1), 63–77. https://doi.org/10.1016/s0040-1951(98)00234-0

Seeman, U., Pumpin, V. F., & Casson, N. (1990). Amposta oil field. In *Proceedings of the AAPG treatise of petroleum geology: Atlas of oil and gas fields, structural traps II: Traps associated with tectonic faulting*. American Association of Petroleum Geologists.

The Corner (2017). Retrieved from http://thecorner.eu/spain-economy/the-castor-project-spaniards-are-paying-for-the-failure-of-this-gas-storage-installation/69669/(29 Dec, 2017) (accessed on 25 Feb 2019).

Vilarrasa, V., & Carrera, J. (2015). Reply to Zoback and Gorelick: Geologic carbon storage remains a safe strategy to significantly reduce CO2 emissions. *Proceedings of the National Academy of Sciences of the United States of America*, *112*(33), E4511. https://doi.org/10.1073/pnas.1511302112

Vilarrasa, V., & Carrera, J. (2015). Geologic carbon storage is unlikely to trigger large earthquakes and reactivate faults through which CO_2 could leak. *Proceedings of the National Academy of Sciences of the United States of America*, *112*(19), 5938–5943. https://doi.org/10.1073/pnas.1413284112

Vilarrasa, V., Carrera, J., Olivella, S., Rutqvist, J., & Laloui, L. (2019). Induced seismicity in geologic carbon storage. *Solid Earth*, *10*, 871–892. https://doi.org/10.5194/se-10-871-2019

Vilarrasa, V., De Simone, S., Carrera, J., & Villaseñor, A. (2020). *Data on the numerical simulations of the induced seismcity at the Amposta fault. Institutional repository DIGITAL*. CSIC. Retrieved from https://digital.csic.es/handle/10261/216863

Villaseñor, A., Herrmann, R. B., Gaite, B., & Ugalde, A. (2020). Fault reactivation by gas injection at an underground gas storage off the east coast of Spain. *Solid Earth*, *11*, 63–74. https://doi.org/10.5194/se-11-63-2020

Wei, S., Avouac, J.-P., Hudnut, K. W., Donnellan, A., Parker, J. W., Graves, R. W., et al. (2015). The 2012 Brawley swarm triggered by injection-induced aseismic slip. *Earth and Planetary Science Letters*, *422*, 115–125. https://doi.org/10.1016/j.epsl.2015.03.054

Zoback, M. D., & Gorelick, S. M. (2015). To prevent earthquake triggering, pressure changes due to CO_2 injection need to be limited. *Proceedings of the National Academy of Sciences of the United States of America*, *112*(33), E4510. https://doi.org/10.1073/pnas.1508533112